Scanning holographic microscopy with spatially incoherent sources: reconciling the holographic advantage with the sectioning advantage

Guy Indebetouw

Physics Department, Virginia Tech, Blacksburg, Virginia 24061-0435, USA (gindebet@vt.edu)

Received August 7, 2008; revised November 14, 2008; accepted December 4, 2008;
posted December 11, 2008 (Doc. ID 99953); published January 20, 2009

A new mode of operation of scanning holographic microscopy that combines the two seemingly incompatible holographic advantage and axial sectioning advantage is proposed and demonstrated. Temporally modulated Fabry–Perot fringes are scanned in a two-dimensional raster over the specimen. With a spatially coherent (point) source, the fringes are spatially nonlocalized and encode the entire three-dimensional volume of the specimen in the form of a single-sideband in-line Fresnel hologram. With an extended spatially incoherent source the fringes are axially localized and select the modulated information from a specific axial plane only. The holographic advantage and the sectioning advantage can thus be achieved with the same scanning holographic setup using different source sizes. © 2009 Optical Society of America

OCIS codes: 090.1995, 110.6880, 180.0180, 180.6900.

1. INTRODUCTION

Two apparently conflicting aims have driven recent developments of new microscopy modalities. The study of dynamical cellular activities, for example, requires the capture of three-dimensional specimen volumes with both rapid acquisition time and high axial resolution. The two aims appear to be mutually exclusive. On the one hand, holography offers the evident advantage of capturing a three-dimensional volume in a single acquisition step. The reconstructed three-dimensional information may, however, be corrupted by the out-of-focus haze that also plagues standard wide field microscopy. Confocal sectioning, on the other hand, acquires the information from a single axial plane exclusively, thus avoiding the out-of-focus haze. However, sectioning methods require a point-by-point sequential acquisition of a number of axial planes and are inherently slow. It thus appears that way because they are based on such different conjectures; the holographic advantage and the sectioning advantage cannot be reconciled using a single technique.

The aim of this paper is to present preliminary results showing that both the holographic and the sectioning advantages can be obtained simultaneously with the method of scanning holographic microscopy. This paper is organized as follows. Since works on holographic microscopy and on sectioning methods are abundantly documented in the literature, only a succinct background is given in Section 2. A new mode of operation of scanning holographic microscopy using Fabry–Perot fringes with both spatially coherent and spatially incoherent sources is described in Section 3. The experimental results presented in Section 4 show that the scanning holographic technique can capture three-dimensional distributions holographically when using a spatially coherent source and also capture single axial sections selectively when using a broad spatially incoherent source. A summary and discussions are given in Section 5.

2. BACKGROUND

A. Digital Holography

During the past decades, digital holography [1,2] has experienced a rapid revival due in part to technological advances in high resolution detectors [CCD and complementary metal-oxide semiconductor (CMOS arrays)], easy access to inexpensive digital memory, and powerful digital processing. Several forms of digital holography have been applied with success to three-dimensional microscopy. A brief account is given in this section. The most common arrangement of digital holography is based on the coherent recording of an object wavefront by interference with an off-axis reference wave. Its application to microscopy has led to impressive results. [3]. In addition to providing holograms of three-dimensional coherently scattered light distributions, the method gives access to a quantitative measure of the phase of the reconstructed wavefront. With biological specimens, the phase gives information on the refractive index and thickness distributions, which in turn are related to biomasses, density, etc. [4,5]. Off-axis digital holographic microscopy requires carefully controlled reconstruction algorithms, not only to extract the reconstruction from the zero order and the twin image but also to compensate for the phase distortions and aberrations inherent to the geometry of the setup [6–8]. Other forms of digital holographic microscopy have also been developed. For example, in-line holography, which is close to the original idea of Gabor [9], has been shown to avoid the twin image problem by using a

single point source close to the hologram plane [10,11]. The method is best suited for recording holograms of dilute distributions of scatterers, but because of its simple and robust setup, relaxed requirements on source coherence and detector spatial resolution, as well as a straightforward reconstruction algorithm, digital in-line holographic microscopy has been useful in capturing holograms in harsh environments [12–14] or using radiations other than visible light [15].

In off-axis digital holography, the hologram is recorded as an interference pattern on a high spatial resolution detector. Although the resolution of electronic imaging detectors keeps improving with time, it still remains a major limiting factor in digital holographic microscopy. Furthermore, interferometric methods require a minimum degree of spatial and spectral (temporal) coherence of the radiation. This limits their use to recording coherently scattered fields and precludes their applications to the holographic recordings of incoherently scattered fields, such as fluorescence or luminescence distributions.

A form of incoherent holography had been suggested [16] as a spinoff of the so called two-pupil-interaction method invented to process incoherent images with complex point-spread-functions [17]. Applied to holographic microscopy, the method has the advantage of being able to capture holograms of incoherently scattered (e.g., fluorescent) light fields. This advantage is crucial in modern biological investigations at the cellular level that rely heavily on the use of specific fluorophores to tag and track the functionalities of specific organelles. Relaxing the coherence requirement of conventional holography has of course a price to pay for. The phase needed to reconstruct the three-dimensional object cannot be captured interferometrically in the spatial domain but must be captured in the temporal domain. This can be achieved by either heterodyne techniques [18–20] or homodyne techniques [21] using phase-shifting methods [22]. In either case, the price to pay is that one two-dimensional raster scan is needed to capture the phase of the hologram of a three-dimensional object in the temporal domain. In spite of this drawback, scanning holographic microscopy has two important advantages. The first is that the method uses either point detectors or spatially integrating detectors. This eliminates the spatial resolution requirement of imaging detectors. The second advantage is that scanning holographic microscopy cannot only capture holograms of incoherently scattered fields but can also yield quantitative phase information [23]. With a spatially integrating detector, the method operates in an incoherent mode, and the hologram is that of a three-dimensional intensity or fluorescence distribution. With a point detector, the method operates in a coherent mode, and the resulting hologram is that of a complex amplitude distribution from which quantitative phase information can be obtained [23,24]. More recently, a different form of incoherent holography has demonstrated the possibility of recording Fresnel holograms of fluorescent distributions without scanning [25,26]. The method, which is based on wide field imaging and thus requires a high resolution imaging detector, uses complex pupils encoded on a spatial light modulator and phase stepping methods to extract the phase information.

B. Axial Sectioning

The challenge in wide field microscopy has been to overcome an out-of-focus haze. The low spatial frequency background of out-of-focus features is always transmitted by the objective and cannot be separated directly from the focused image of interest. Two diametrically opposite approaches have been successful in combating this problem. The first is to record all the photons of the wide field image and redistribute the out-of-focus light by postprocessing deconvolution [27]. These methods have the advantage of capturing large signals and the disadvantage of having to rely on iterative digital algorithms to extract the desired information. The second approach to eliminating the out-of-focus haze is to exclude the out-of-focus light from the detector in the first place. This requires a point-to-point three-dimensional scanning of the specimen using confocal pinholes. The out-of-focus light rejection is straightforward, but the method is slow, and, in practice, the detected signal may be so low as to require opening the pinhole size to obtain an adequate signal-to-noise ratio at the expense of spoiling the resolution [28]. Comparative evaluations of the two methods [29,30] lead to the conclusion that which is best depends entirely on the type of specimen studied and its environmental conditions [31].

A third approach to axial sectioning with wide field imaging, which was developed more recently, makes use of structured illumination. The idea is to shift the undesirable low spatial frequencies of out-of-focus features away from the objective's transmission peak or to redistribute them in such a way that they can be eliminated statistically. The method is elegantly simple, but extracting axial sections requires the acquisition and digital manipulation of several frames. The grid projection method [32,33] requires three or more frames with precise stepping of the grid while the speckle projection method [34] requires at least ten frames with different speckle fields for adequate statistical processing. Because they are easy to implement, sectioning methods with structured illumination are increasing in popularity.

3. SCANNING HOLOGRAPHIC MICROSCOPY WITH SPATIALLY INCOHERENT SOURCES

A. General Description

Scanning holographic microscopy has been described in previous publications [19,23,24,35]. In this method, a temporally modulated interference pattern is raster scanned over the specimen to encode its three-dimensional distribution. Most applications described so far were aimed at obtaining single-sideband in-line holograms of three-dimensional fluorescent distributions. For this, the scanning pattern was a Fresnel zone pattern created by the interference of a plane wave and a spherical wave with a temporal frequency shift between them [24]. The entire scattered or fluorescent light is captured by a nonimaging detector. After demodulation, the signal represents a single-sideband Fresnel hologram in which each scatterer is encoded as a spherical wave with a radius of curvature equal to its axial position. The use of a Fresnel scanning pattern produced by a two-beam interferometer

is convenient and simple but not necessary nor unique. Indeed, it has been suggested that different scanning distributions could be exploited to synthesize arbitrary complex point-spread-functions [36].

In this paper, the scanning pattern is created by the fringes of a Fabry–Perot interferometer. The reason for this choice is that Fabry–Perot fringes can be obtained either with a spatially coherent source (a diverging or converging spherical wave from a point source) or with an extended spatially incoherent source (arc lamps, light emitting diodes, or dynamic diffusers). The temporal modulation of the interference fringes is obtained by scanning the Fabry–Perot interferometer. It should be mentioned that the Fabry–Perot need not have a high finesse because, as will be explained in Subsection 3.B, it is effectively used as a two-beam interferometer. The key idea is that with a spatially coherent source, the fringes are not localized in space. Consequently, all the scatterers or fluorophores distributions of the three-dimensional specimen are encoded in a single two-dimensional scan. This results in the formation of a hologram similar to that obtained with the original two-beam or two-pupil setup. With an extended spatially incoherent source, the fringes are localized in a specific axial plane, coinciding with the focal plane of the objective. As a result, only the scatterers or fluorophores located in that particular axial plane are encoded and contribute to the temporally modulated signal. Out-of-focus features produce a stationary background that may or may not tax the dynamic range of the detector but does not contribute to the image of the selected axial section.

The axial sectioning operation achieved by this method is different from that obtained with structured illumination methods and confocal methods. Structured illumination methods attempt to correct the fact that the incoherent optical transfer function always acts as a low-pass filter and as a strongly low-pass filter for out-of-focus information. This is the source of the out-of-focus haze. In contrast, the transfer function in scanning holography is the coherent transfer function of the objective, whether the method is used in the coherent or the incoherent mode [24]. All spatial frequencies are thus always transmitted with a transmission factor of 1, but the spectra of out-of-focus features acquire quadratic phase factors [37]. This fact has been exploited to design *a posteriori* processing algorithms for the extraction of axial sections from the reconstruction of scanning holograms [38,39]. It means however that shifting the spatial frequency spectrum as is done with structured illumination would be ineffective in scanning holography. The only way to achieve axial sectioning, other than using *a posteriori* processing, is to select the desired information at the detection stage. In confocal methods, the point-to-point selection of an axial section relies on the rejection of all the other volumetric information away from the detector. The method is indeed effective but often results in very low signal levels. In contrast, the present method captures the entire scattered or fluorescent signal excited by the scanning pattern. The signal has therefore always a high instantaneous level, but the axial localization of the fringe pattern ensures that only the signal pertaining to a specific axial plane is modulated and contributes to the image of that section.

To summarize, scanning holography using a Fresnel scanning pattern created by the interference of two beams issued from a point pupil and a pupil with a spherical distribution operates in an incoherent mode with a spatially integrating detector or in a coherent mode with a point detector located in a conjugate plane of the point pupil. The mode of operation described in this paper may be dubbed the tomographic mode. Holograms of single axial sections are obtained using a Fresnel scanning pattern localized in a specific axial plane. In the method described here, the localized fringes are obtained with an extended spatially incoherent source and a Fabry–Perot interferometer. This method does not access quantitative phase information unless a point source is used instead of an extended source. With an extended source, the coherent mode and tomographic modes are mutually exclusive. It is however possible to obtain localized fringes with a point source and a two-beam interferometer if the source is of low temporal coherence. The use of a supercontinuum source, for example, raises the interesting prospect of accessing the phase of a single axial section of a specimen, and obtaining tomographic imaging of three-dimensional refractive index distributions.

B. Theoretical Analysis

A brief theoretical account is given in this section with reference to the setup sketched in Fig. 1. The source is either a single point source, used to record a hologram, or an extended spatially incoherent source, used to capture individual axial sections. In either case, the analysis starts with the determination of the scanning pattern created in object space by a single point source. As shown in Fig. 1, a point source illuminates the Fabry–Perot with a spherical wave that is collimated by lens L_1. Multiple reflections in the Fabry–Perot duplicate this point in a series of images axially spaced by twice the mirror spacing. The interference of the waves from these multiple sources gives a characteristic pattern of rings in the back focal plane of lens L_1. Lens L_2 forms an image of the Fabry–Perot to fill the pupil of the microscope objective. The ring pattern is imaged on the specimen, through the objective, with a demagnification f_0/f_2, where f_0 is the focal length of the objective and f_2 is that of lens L_2. For a point source on axis, the complex amplitude distribution in the pupil plane of the objective can be written as

$$\tilde{P}(\vec{\rho},z) = (1-R)^2\left[\delta(\vec{\rho}) + \sum_n \exp(\mathrm{in}\Omega t)\tilde{P}_n(\vec{\rho},z)\right]\mathrm{Disc}(\rho/\rho_{\mathrm{MAX}}), \tag{1}$$

where $\vec{\rho}$ is the spatial frequency coordinate in the pupil of the objective, R is the reflection coefficient of the Fabry–Perot mirrors, Ω is the Doppler frequency shift due to the mirror translation, ρ_{MAX} is the cutoff frequency of the objective, n is a positive integer, and $\tilde{P}_n(\rho,z)$ is the spherical wave due to the nth reflection in the Fabry–Perot. Using the generalized pupil description [40] we have, in the paraxial approximation,

$$\tilde{P}_n(\rho,z) = R^n \exp(i4\pi nd/\lambda)\exp[(i\pi/n)\lambda(z_0+z)\rho^2], \tag{2}$$

where $z_0=(f_0f_1/f_2)^2/2d$ and d is the mirror spacing of the Fabry–Perot.

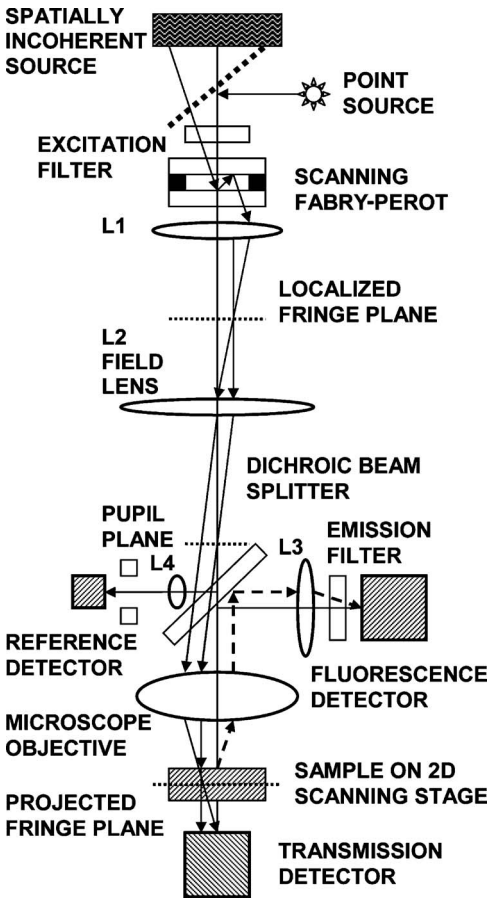

Fig. 1. Sketch of the scanning holographic microscopy setup using a Fabry–Perot interferometer to create the Fresnel scanning pattern. With a point source, the fringes are not localized and lead to the recording of a hologram. With an extended incoherent source, the fringes are axially localized in the focal plane of the objective and lead to the recording of a single axial section. For the results of Section 4, the objective was a Mytutoyo 20 $\times$0.4 NA with a focal length of 1 cm, and the lenses had focal lengths $f_1=5$ and $f_2=60$ cm.

The axial coordinate z in object space is measured from the focal plane of the objective. In that focal plane, the wave transmitted directly through the Fabry–Perot and focused at the pupil center [the first term in the bracket in Eq. (1)] becomes a plane wave. The first reflected wave ($n=1$) becomes a spherical wave with a radius of curvature z_0 and a transverse radius a. To take full advantage of the resolution of the microscope objective, the numerical aperture of the pattern should match that of the objective, namely, $a=\mathrm{NA}\ z_0$.

The scanning pattern amplitude in object space is the two-dimensional inverse Fourier transform of the pupil distribution given by Eq. (1). The raster scan affects a convolution of the object intensity distribution with the scanning pattern intensity. The modulated signal is collected by a spatially integrating detector, bandpass filtered around the modulation frequency Ω created by the translation of one of the Fabry–Perot mirrors, and rearranged in a two-dimensional format. The Fourier transform of the resulting single-sideband hologram has the form

$$\tilde{H}(\vec{\rho}) = \int \mathrm{d}z \tilde{S}_\Omega(\rho,z)\tilde{I}(\vec{\rho},z), \tag{3}$$

where $\tilde{I}(\vec{\rho},z)$ is the two-dimensional Fourier transform of the z-section of the specimen, and

$$\tilde{S}_\Omega(\rho,z) = \left[\tilde{P}_1(\rho,z) + \sum_n \tilde{P}_{n+1}(\rho,z) * \tilde{P}_n^*(\rho,z)\right]\mathrm{Disc}(\rho/\rho_{\mathrm{MAX}}) \tag{4}$$

is the two-dimensional Fourier transform of the sum of all terms in the scanning distribution that are modulated at the frequency Ω. The centered asterisk represents a convolution integral and the asterisk a complex conjugate. Using Eq. (2), it can be shown that Eq. (4) reduces to the simple form

$$\tilde{S}_\Omega(\rho,z) = A\exp(i4\pi d/\lambda)\exp[i\pi\lambda(z_0+z)\rho^2]\mathrm{Disc}(\rho/\rho_{\mathrm{MAX}}), \tag{5}$$

where $A=R(1+\Sigma_n R^{2n+1})$ is a constant and $\mathrm{Disc}(x)=1$ for $x<1$ and zero otherwise.

Note that the first term in Eq. (4) is identical to the spherical wave encoding each object point in the original two-wave interference setup [19]. The additional terms are due to multiple-beam interference. The important point is that all the terms oscillating at frequency Ω have the same spherical curvature. This means that the multiple-beam interference terms do not introduce any additional phase distortions or aberrations. The demodulated signal is thus equivalent to the signal obtained with a two-beam setup except for an unimportant constant factor. Because of this, the reconstruction of the hologram can be carried out the usual way by free-space propagation to a chosen reconstruction plane $z=z_R$. In Fourier space, this is expressed by multiplying the Fourier transform of the hologram with the free-space transfer function $\exp[-i\pi\lambda(z_0+z_R)\rho^2]$.

Equivalently, the reconstruction can be accomplished by a correlation of the hologram with the two-dimensional section of the scanning distribution in plane z_R. The latter can be recorded experimentally as the hologram of a subresolution point object. As has been shown before, this method allows for full compensation of the aberrations of the optics [35].

When the source is spatially coherent (a single point source), the rings of the scanning distribution are nonlocalized and the entire three-dimensional specimen distribution is recorded in the form of a single-sideband Fresnel hologram. The Fourier transform of the reconstructed image focused in plane z_R has the final form

$$\tilde{R}^{\mathrm{COH}}(\vec{\rho},z,z_R) = \int \mathrm{d}z\tilde{I}(\vec{\rho},z)\exp[i\pi\lambda(z-z_R)\rho^2]\mathrm{Disc}(\rho/\rho_{\mathrm{MAX}}), \tag{6}$$

which is identical to the reconstruction in the two-beam method [24].

With an extended spatially incoherent source, the previous analysis is still valid, but the scanning pattern is now the incoherent superposition of the contributions from each individual point source. As a result, the Fabry–

Perot ring pattern is localized in the back focal plane of lens L_1, and its projection in object space is axially localized in the focal plane of the objective because this is the only plane where the interference rings due to different point sources are exactly superposed. In Eqs. (3) and (4), the scanning distribution must be multiplied by a delta function $\delta(z)$, and the final reconstruction is, in Fourier space,

$$\tilde{S}^{\mathrm{INCOH}}(\vec{\rho},z) \approx \tilde{I}(\vec{\rho},0)\delta(z)\mathrm{Disc}(\rho/\rho_{\mathrm{MAX}}). \tag{7}$$

This represents the Fourier transform of a single section of the specimen without out-of-focus haze. Equation (7) is an approximation. As will be shown in a future publication, the axial depth of localization of the Fabry–Perot rings is

$$\Delta z = \lambda/[(\sin\alpha)(\sin\beta)], \tag{8}$$

where α is the angular size of the pupil ($\sin\alpha$ is the numerical aperture of the objective) and β is the angular size of the incoherent source projected in the pupil plane. There are two limiting cases. With a point source ($\beta\rightarrow 0$), the fringes are not localized and encode the entire three-dimensional object distribution in the form of a hologram. With an extended spatially incoherent source filling entirely the pupil of the objective ($\beta \geqslant \alpha$), the fringes are axially localized within an axial depth equal to the depth-of-focus of the objective ($\lambda/(\sin\alpha)^2$). The resulting section represents a slab of the specimen with a thickness equal to the depth-of-focus of the objective.

4. EXPERIMENTAL RESULTS

A. Setup

The experimental setup is sketched in Fig. 1. The Fabry–Perot interferometer consists of two partially reflecting plane mirrors (reflection coefficient ~60%). One of the mirrors is mounted onto a piezoelectric linear translator. Since the purpose of these experiments is to demonstrate the soundness of the proposed method, rather than optimize its properties, we chose a laser (DPSS 532 nm) to produce the point source. The same laser that expanded and scattered on a dynamic diffuser (a spinning ground glass) was used as an extended spatially incoherent source. The rationale for this choice was that using the same setup and the same excitation wavelength for the holographic recording and the axial sectioning would provide a fair comparison of the two modes of operation. The use of a laser is however not necessary. Spectral lamps and LEDs are inexpensive and offer extended wavelength diversity. The spectral coherence requirement for the source is that its linewidth should be smaller than the free-spectral-range of the Fabry–Perot, which is equivalent to requiring a source with a coherence length larger than twice the mirror spacing.

B. Results

The experiment is aimed at comparing the holographic reconstruction with the sectioning reconstruction using the same scanning holographic microscope setup, only with different source sizes. For this, the specimen was a homemade slide of fluorescent beads (DukeR0200, 2 μm in diameter, excitation ~542 nm, emission ~612 nm). The beads tend to stick to the top surface of the mounting slide and to the bottom surface of the coverslip. This provides a simple three-dimensional test sample. In the sample used, the distance between the two planes was ~35 μm. For the experiment, the mirror spacing was ~5 mm. The microscope objective was a Mitutoyo 20 $\times$0.4 NA with a focal length of 10 mm. Lenses L_1 and L_2 had focal lengths of 5 and 60 cm, respectively. The plane of the Fabry–Perot is imaged in the pupil plane of the objective with a magnification of 20$\times$, and the Fabry–Perot fringes localized in the focal plane of lens $L1$ are imaged in the focal plane of the objective with a magnification of 1/60$\times$.

The linear translation of the Fabry–Perot mirror resulted in a fringe modulation frequency of ~10 kHz, and the data acquisition rate was 50 kHz to satisfy the Shannon–Nyquist theorem.

The holographic mode of operation is obtained using a point source. The ring pattern in object space had a radius of ~35 μm and a Fresnel number of ~16, which corresponds to a radius of curvature $z_0 \sim 140$ μm. The effective numerical aperture of the holographic microscope was thus ~0.25. A reference hologram of a 0.5 μm pinhole located in the focal plane of the objective was recorded in order to reconstruct the specimen hologram by correlation and thus cancel the spherical aberration of the optics. Note that this reference hologram needs to be recorded only once for a given scanning pattern. The reconstruction focused in an arbitrary plane $z=z_R$ is obtained by propagating the reference hologram for a distance z_R using Fresnel propagation and correlating the hologram of the specimen with the propagated reference hologram.

Figure 2 shows the holographic reconstructions focused in the two planes containing most of the beads ($z_1=-15$ and $z_2=+20$ μm). We can clearly distinguish different beads in focus in the two different planes. However, we also see that these reconstructions are severely degraded by the presence of the out-of-focus images. This result demonstrates the holographic advantage, which is to capture the entire three-dimensional holographic volume in a single acquisition step. It also illustrates how severely the out-of-focus information can degrade the reconstructed images of certain types of specimens. To clear up a series of reconstructions in different axial planes would require applying *a posteriori* processing with deconvolution algorithms.

Single axial sections were recorded with the same setup but with the point source replaced by an extended incoherent source (an extended beam scattered by a dynamic diffusor). To avoid spurious reflection in the objective, the source diameter was ~0.8 times the pupil diameter. From Eq. (8), the expected axial resolution of an axial section is thus ~10 μm. Individual sections were obtained by bringing the desired section in focus in the plane of localization of the fringes and correlating the resulting single-section hologram with the hologram of the 0.5 μm pinhole located in the focal plane of the objective, where the fringes are localized. Figure 3 shows the two sections obtained with the fringes localized in the planes $z=-15$ and $z=20$ μm. The different beads in focus in each plane are now clearly visible without the disturbance of

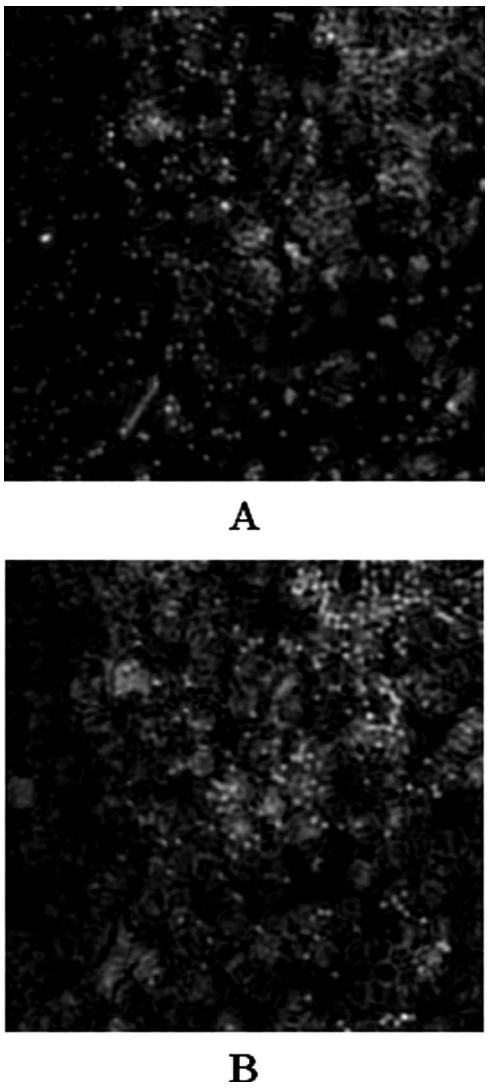

Fig. 2. Reconstructions of the hologram of a dense sample of 2 μm diameter fluorescent beads. The reconstructions are focused in the two planes where most of the beads are located: $z=-15$ and $z=20$ μm. The field is 140×140 μm. The hologram has captured the entire three-dimensional field, but the reconstructions are severely corrupted by the out-of-focus information.

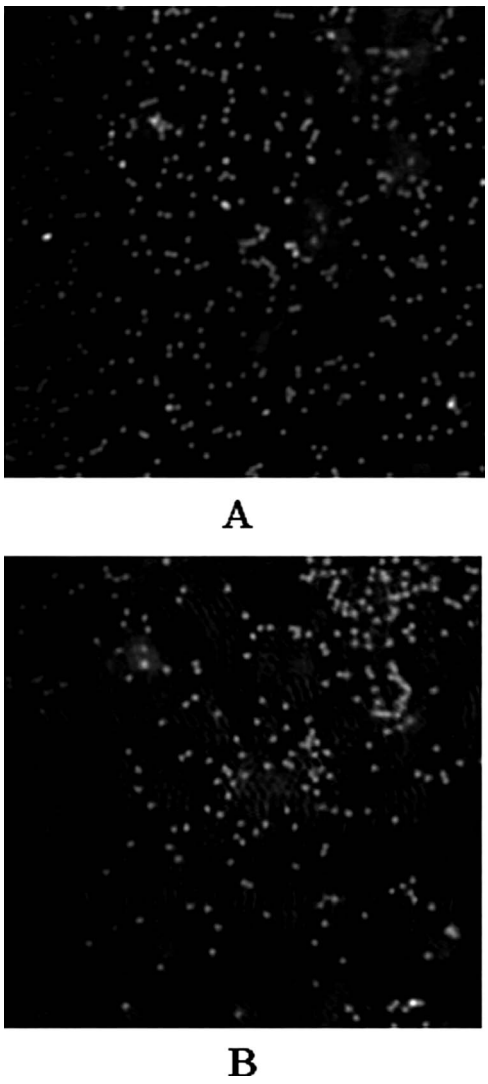

Fig. 3. Axial sections of the same two planes as shown in Fig. 2 obtained with an extended spatially incoherent source producing an axially localized scanning Fresnel fringe pattern and leading to the hologram of a single axial section without the disturbance of the out-of-focus information.

the out-of-focus information. This result demonstrates the sectioning advantage of scanning holography, which is to select the information from a single axial section for each acquisition step.

5. SUMMARY

A new method of operation of scanning holographic microscopy has been analyzed and demonstrated experimentally. Previously described modes of operation of scanning holography were using a spatially coherent (point) source to create the temporally modulated Fresnel fringe pattern that scans the specimen and encodes its three-dimensional scattering distribution. This fringe pattern was conveniently produced by the two-beam interference of a plane wave and a spherical wave, issued, respectively, from a point pupil and a quadratic phase pupil. With a point source, scanning holography can operate in an incoherent mode if the signal is captured by an extended spatially integrating detector or in a coherent mode if the signal is captured by a point detector in an image plane of the point pupil. The incoherent mode of operation gives a hologram of the incoherently scattered intensity distribution of the specimen (e.g., fluorescence) while the coherent mode of operation gives a hologram of the complex amplitude of the specimen from which quantitative phase can be measured.

The new mode of operation described here uses a Fabry–Perot to create the scanning Fresnel fringe pattern. With a point source, this mode of operation gives holograms identical to the holograms obtained with the two-beam method. With an extended incoherent source, the Fabry–Perot fringes are axially localized in the focal plane of the objective and select the scattered information from that specific axial section only. This provides a new means of accessing axial information selectively and rejecting the out-of-focus information. Scanning holographic microscopy provides thus a means of exploiting both the

holographic advantage and the sectioning advantage, as well as accessing both coherently and incoherently scattered information.

REFERENCES

1. J. W. Goodman and R. W. Lawrence, "Digital image formation from electronically detected holograms," Appl. Phys. Lett. **11**, 77–79 (1967).
2. M. A. Kronrod, N. S. Merzlyakov, and L. P. Yaroslawskii, "Reconstruction of a hologram with a computer," Soviet Phys.-Techn. Phys. **17**, 333–334 (1972).
3. B. Rappaz, P. Marquet, E. Cuche, Y. Emery, C. Depeursinge, and P. J. Magistretti, "Measurement of the integral refractive index and dynamic cell morphometry of living cell with digital holographic microscopy," Opt. Express **13**, 9361–9373 (2005).
4. E. Cuche, F. Bevilaqua, and C. Depeursinge, "Digital holography for quantitative phase-contrast imaging," Opt. Lett. **24**, 291–293 (1999).
5. P. Marquet, B. Rappaz, P. Magistretti, E. Cuche, Y. Emery, T. Colomb, and C. Depeursinge, "Digital holographic microscopy: a noninvasive contrast imaging technique allowing quantitative visualization of living cell with subwavelength axial accuracy," Opt. Lett. **30**, 468–470 (2005).
6. E. Cuche, P. Marquet, and C. Depeursinge, "Simultaneous amplitude-contrast and quantitative phase-contrast microscopy by numerical reconstruction of Fresnel off-axis holograms," Appl. Opt. **38**, 6994–7001 (1999).
7. D. Carl, B. Kemper, G. Wernicke, and G. von Bally, "Parameter-optimized digital holographic microscope for high-resolution living-cell analysis," Appl. Opt. **43**, 6536–6543 (2005).
8. P. Picart and J. Leval, "General theoretical formulation of image formation in digital Fresnel holography," J. Opt. Soc. Am. A **25**, 1744–1760 (2008).
9. D. Gabor, "A new microscopic principle," Nature **4098**, 777–778 (1948).
10. O. Ersoy, "One-image-only digital holography," Optik (Jena) **53**, 47–62 (1979).
11. J. Garcia-Sucerquia, W. Xu, S. K. Jericho, P. Klayes, M. H. Jericho, and H. J. Kreuzer, "Digital in-line holographic microscopy," Appl. Opt. **45**, 836–850 (2006).
12. R. B. Owen and A. A. Zozulya, "In-line digital holgraphic sensor for monitoring and characterizing marine particulates," Opt. Eng. (Bellingham) **38**, 2187–2197 (2000).
13. J. Watson, S. Alexander, G. Crayg, D. C. Hendry, P. R. Hobson, R. S. Lampitt, J. M. Marteau, H. Hareid, M. A. Player, K. Saw, and K. Tipping, "Simultaneous in-line and off-axis subsea holographic recording of plankton and other marine particles," Meas. Sci. Technol. **12**, L9–L15 (2001).
14. S. K. Jericho, J. Garcia-Sucerquia, W. Xu, M. H. Jericho, and H. J. Kreuzer, "Submersible digital in-line holographic microscope," Rev. Sci. Instrum. **77**, 043706 (2006).
15. H. J. Kreuzer, M. J. Jericho, I. A. Meinertzhagen, and W. Xu, "Digital in-line holography with photons and electrons," J. Phys. Condens. Matter **36**, 10729–10741 (2001).
16. T.-C. Poon and A. Korpel, "Optical transfer function of an acousto-optic heterodyning image processor," Opt. Lett. **4**, 317–319 (1979).
17. A. W. Lohmann and W. T. Rhodes, "Two-pupil synthesis of optical transfer functions," Appl. Opt. **17**, 1141–1150 (1978).
18. B. Schilling, T.-C. Poon, G. Indebetouw, B. Storrie, K. Shinoda, and M. Wu, "Three-dimensional holographic fluorescence microscopy," Opt. Lett. **22**, 1506–1508 (1997).
19. G. Indebetouw and W. Zhong, "Scanning holographic microscopy of three-dimensional fluorescent specimens," J. Opt. Soc. Am. A **23**, 1699–1707 (2006).
20. G. Indebetouw, Y. Tada, R. Rosen, and G. Brooker, "Scanning holographic microscopy with resolution exceeding the Rayleigh limit of the objective by superposition of off-axis holograms," Appl. Opt. **46**, 993–1000 (2007).
21. J. Rosen, G. Indebetouw, and G. Brooker, "Homodyne scanning holography," Opt. Express **14**, 4280–4285 (2006).
22. I. Yamaguchi and T. Zhang, "Phase-shifting digital holography," Opt. Lett. **22**, 1268–1270 (1997).
23. G. Indebetouw, Y. Tada, and J. Leacock, "Quantitative phase imaging with scanning holographic microscopy: an experimental assessment," Biomed. Eng. Online **5**:63, 1–7 (2006).
24. G. Indebetouw, P. K. Klysubun, T. Kim, and T.-C. Poon, "Imaging properties of scanning holographic microscopy," J. Opt. Soc. Am. A **17**, 380–390 (2000).
25. J. Rosen and G. Brooker, "Digital spatially incoherent Fresnel holography," Opt. Lett. **32**, 912–914 (2007).
26. J. Rosen and G. Brooker, "Non-scanning motionless fluorescence three-dimensional holographic microscopy," Nat. Photonics **2**, 190–195 (2008).
27. P. Sarder and A. Nehorai, "Deconvolution methods for 3-D fluorescence microscopy images: an overview," IEEE Signal Process. Mag. **23**, 32–45 (2006).
28. E. H. K. Stelzer, "Contrast, resolution, pixelation, dynamic range and signal-to-noise ratio: fundamental limits to resolution in fluorescence light microscopy," J. Microsc. **189**, 15–24 (1997).
29. P. J. Verveer, M. J. Gemkow, and T. M. Jovin, "A comparison of image restoration approaches applied to three-dimensional confocal and wide-field fluorescence microscopy," J. Microsc. **193**, 50–61 (1999).
30. P. J. Shaw, "Comparison of wide-field/deconvolution and confocal microscopy for 3D imaging," in *Handbook of Biological Confocal Microscopy*, J. B. Pawley, ed. (Plenum, 1995). pp.373–387
31. J. R. Swedlow, K. Hu, P. D. Andrews, D. S. Roos, and J. M. Murray, "Measuring tubulin content in toxoplasma gondii: a comparison of laser-scanning confocal and wide-field fluorescence microscopy," Proc. Natl. Acad. Sci. U.S.A. **99**, 2014–2019 (2002).
32. M. A. A. Neil, R. Justaikis, and T. Wilson, "Method of obtaining optical sectioning by using structured light in a conventional microscope," Opt. Lett. **22**, 1905–1907 (1997).
33. M. A. A. Neil, A. Squire, R. Justaikis, P. I. H. Bastiaens, and T. Wilson, "Wide-field optically sectioning fluorescence microscopy with laser illumination," J. Microsc. **197**, 1–4 (1999).
34. C. Ventalon and J. Mertz, "Dynamic speckle illumination microscopy with translated versus randomized speckle patterns," Opt. Express **14**, 7198–7209 (2006).
35. G. Indebetouw, A. El Maghnouji, and R. Foster, "Scanning holographic microscopy with transverse resolution exceeding the Rayleigh limit and extended depth of focus," J. Opt. Soc. Am. A **22**, 892–898 (2005).
36. G. Indebetouw, W. Zhong, and D. Chamberlin-Long, "Point-spread-function synthesis in scanning holographic microscopy," J. Opt. Soc. Am. A **23**, 1708–1717 (2006).
37. G. W. Goodman, *Introduction to Fourier Optics* (McGraw-Hill, 1988).
38. T. Kim, "Optical sectioning by optical scanning holography and a Wiener filter," Appl. Opt. **45**, 872–879 (2006).
39. G. Indebetouw, "*A posteriori* quasi-sectioning of the three-dimensional reconstructions of scanning holographic microscopy," J. Opt. Soc. Am. A **23**, 2657–2661 (2006).
40. C. W. McCutchen, "Generalized aperture and the three-dimensional diffraction image," J. Opt. Soc. Am. **54**, 240–244 (1964).